Supporting Information

Self-Synergistic Cobalt Catalysts with Symbiotic Metal Single-Atoms and Nanoparticles for Efficient Oxygen Reduction

Wu Zhou,[1,#] Hui Su,[2,#] Zijun Wang,[1] Feng Yu,[1] Wei Wang,[1,*] Xin Chen,[3,*] and Qinghua Liu[2,*]

[1]*School of Chemistry and Chemical Engineering, Key Laboratory for Green Processing of Chemical Engineering of Xinjiang Bingtuan, Shihezi University, Shihezi 832003, China*

[2]*National Synchrotron Radiation Laboratory, University of Science and Technology of China, Hefei 230029, Anhui, P. R. China*

[3]*Center for Computational Chemistry and Molecular Simulation, College of Chemistry and Chemical Engineering, Southwest Petroleum University, Chengdu 610500, China*

#These authors contribute equally to this work.

*E-mail: wangw@shzu.edu.cn; chenxin830107@pku.edu.cn; qhliu@ustc.edu.cn

Chemicals

Cobalt nitrate hexahydrate (Co $(NO_3)_2 \cdot 6H_2O$, Sinopharm Chemical Reagent Co.,Ltd, 99%), methanol (CH_3OH, Sinopharm Chemical Reagent Co., Ltd), 2-methylimidazole (Beijing Bailingwei Technology Co., Ltd., 99%), potassium hydroxide (KOH, Sinopharm Chemical Reagent Co., Ltd. >98%), Nafion®117 solution (Sigma-Aldrich.,~5%), Commercial Pt/C catalyst (Aladdin, 20 wt%). All of the chemicals used in this experiment were analytical grade and used without further purification.

Synthesis of ZIF-67

Typically, 0.498 g $Co(NO_3)_2 \cdot 6H_2O$ was dissolved in 50 mL methanol to form a clear and transparent solution A. 0.656 g 2-methylimidazole was added to 50 mL methanol to form homogeneous solution B. Then the solution A was quickly poured into the solution B with vigorous stirring for 10 min, and aged at room temperature for 24 h. The blue-purple sediment was centrifuged at 8000 rpm, washed with methanol several times and dried overnight at 60 ºC to obtain the ZIF-67.

Synthesis of S/Co-SA-NPs and other Co catalysts

In a typical process, the obtained ZIF-67 was thoroughly ground in a mortar, and then 90 mg of ZIF-67 power was sealed in a crucible with a cover and annealed in a muffle furnace at 800 ℃ for 2 h in Ar atmosphere (20 mL/min). The heating process first rises to 350 ℃ at 5 ℃/min and then continues to increase to 800 ℃ at 2 ℃/min. When the temperature in the muffle furnace has cooled to room temperature, the as-prepared samples were further washed with ethanol to remove some impurities and then dried and ground. The catalyst prepared is named S/Co-SA-NPs. The preparation process of Co-SA and Co-NP is similar to S/Co-SA-NPs. The synthesis of Co-SA and Co-NP were achieved by adjusting the heating temperature to 550 ℃ and 950 ℃, respectively. Through temperature control strategy, the Co catalysts with different morphology were successfully synthesized. Moreover, in order to further explore the effect of the synergistic effect of different proportions of Co nanoparticles and Co atoms on the performance of the catalysts, we fine-tuned the temperature of the carbonization process. The catalysts obtained at the carbonization temperature of 700 ℃ and 800 ℃ are named Co-700 and Co-800, respectively.

Characterizations

The field emission scanning electron microscopy (SEM) measurements were performed on JSM-6700F electron microscope at 5 kV. Transmission electron microscopy (TEM), high-resolution transmission electron microscopy (HRTEM) and scanning transmission electron microscopy-energy dispersive spectroscopy (STEM-EDS) were performed on a JEM-2100F microscope at an acceleration voltage of 200 kV. The X-ray diffraction (XRD) patterns were performed on Philips X'Pert Pro Super X-ray diffractometer with Cu Kα radiation; the samples were scanned over the 2θ range from 3 to 80 °. X-ray photoelectron spectroscopy (XPS) data were recorded using a Thermo ESCALAB 250 with Al Kα (hv=1486.6 eV) as the excitation source.

XAFS measurements

The Co *K*-edge XAFS data were collected at BL14W1 station in SSRF (Shanghai Synchrotron Radiation Facility). The storage ring of SSRF was operated at 3.5 GeV with a maximum current of 300 mA. The acquired EXAFS data were processed according to the standard procedures using the ATHENA module implemented in the IFEFFIT software packages. The *k*3-weighted EXAFS spectra were obtained by subtracting the post-edge background from the overall absorption and then normalizing with respect to the edge-jump step. Subsequently, *k*3-weighted χ(k) data in the *k*-space ranging from 2.4–10 $Å^{-1}$ were Fourier transformed to real (R) space using a hanning windows (d*k* = 1.0 $Å^{-1}$) to separate the EXAFS contributions from different coordination shells.

***Operando* SR-FTIR measurements**

The *Operando* synchrotron radiation FTIR data were obtained by measuring on the infrared beamline BL01B of the National Synchrotron Radiation Laboratory (NSRL, China) through a homemade top-plate cell reflection IR setup with a CaF_2 crystal as the infrared transmission window (cutoff energy of ~625cm^{-1}). This end-station was equipped with an FTIR spectrometer (Bruker 66v/s) with a KBr beam splitter and various detectors (herein, a liquid-nitrogen-cooled MCT detector was used) coupled with an IR microscope (Bruker Hyperion 3000) with a 16x objective to provide infrared spectroscopy measurements over a broad range of 15–4000 cm^{-1} and a high spectral

resolution of 0.25 cm^{-1}. The catalyst ink was prepared by dispersing 5 mg of various catalysts into 1 mL of the mixed solvent containing deionized water, ethanol and 5% Nafion with a volumetric ratio of 728: 242: 30. For the preparation of the catalytic electrodes, 30μL of the catalyst ink was loaded onto a foamed Ni electrode to reach a sample loading of ~0.15 mg cm^2. The catalyst electrodes are naturally air-dried at room temperature. In order to reduce the loss of infrared light during in situ infrared testing, the catalyst electrode is pressed tightly against the CaF_2 crystal window with micron gaps. The quality of the SR-FTIR spectrum obtained by adopting the reflection mode of vertically incident infrared light. Each infrared absorption spectrum was acquired by averaging 514 scans at a resolution of 2 cm^{-1}. To ensure the required O_2 in the reaction process, the O_2 saturated KOH solution was circulated through the Kamer micro pump with a flow rate of 100 μL/s. All infrared spectral acquisitions were carried out after a constant potential was applied to the catalyst electrode for 20 min. The background spectrum of the catalyst electrode was acquired at an open-circuit voltage before each systemic ORR measurement, and the measured potential ranges of the ORR were 1.0–0.60 V with an interval of 0.05 V.

***Operando* EIS measurements**

The Operando Electrochemical impedance spectroscopy (EIS) tests were performed with Co catalyst-coated carbon papers in O_2-saturated KOH solution (0.1M) by an electrochemical workstation CHI 760E with a standard three-electrode electrochemical cell. The measured potential ranges of the EIS were 1.0-0.50V (vs RHE) in the frequency range of 0.01-100000 Hz. Before the EIS spectrum was collected at each test voltage, the same voltage was applied to the catalyst electrode for 10 minutes through the i-t test. To ensure full exposure of the active sites, the catalyst ink was prepared by dispersing 5 mg of various catalysts into ~1 mL of the mixed solvent containing 750μL deionized water, 250μL ethanol and 30μL Nafion by continuous ultrasonication for 30 min. 30μL of the catalyst ink was dropcast onto carbon paper as the working electrode to reach a sample loading of ~0.146 mg/cm^2. The carbon paper electrodes were dried at room temperature naturally.

Electrochemical measurements

Electrochemical measurements of ORR performance were carried out on an electrochemical

workstation (Model CHI760E, CH instruments, Inc., Austin, TX) with a standard three-electrode electrochemical cell and was used to record oxygen-involved activity of the samples, where the prepared electrodes immersed in a O_2- or N_2- saturated 0.1 M KOH solution, using a rotating disk electrode (RDE) with an area of 0.071 cm^2 or a rotating ring-disk electrode (RRDE) with an area of 0.196 cm^2 as the working electrode, Ag/AgCl (saturated KCl) as the reference electrode, and Carbon rode as the counter electrode. All potential in the figure was converted to reversible hydrogen electrode (RHE) with the conversion E (vs. RHE) = E (vs. Ag/AgCl) + 0.059×pH + 0.197.

For the electrode preparation process, 5 mg of catalyst powder was dispersed into a mixture solution of 30 μL of Nafion (5 wt%), 250 μL of ethanol, and 750 μL of DI water. And the mixed solution formed the homogeneous catalyst ink under ultrasonic conditions. After that, 5 μL of the dispersion was dripped onto the rotating disk electrode (RDE) (catalyst loading is about 0.34mg/cm^2) and 10 μL catalyst ink was loaded onto the rotating ring-disk electrode (RRDE) (catalyst loading is about 0.34 mg/cm^2).

Prior to the linear sweep voltammetry (LSV) test, the oxygen flow should be pumped into the 0.1m KOH solution for 30min.The LSV tests were measured at various rotating speed from 400 to 2500 rpm with a sweep rate of 10 mV/s. Cyclic voltammetry (CV) curves were evaluated on RDE in O_2-saturated and N_2-saturated solution at a scanning rate of 50 mV/s. The average electron transfer number (n) and kinetic current density (J_k) can be calculated from Koutecky-Levich equations (1):

$$\frac{1}{J} = \frac{1}{J_L} + \frac{1}{J_K} = \frac{1}{B\omega^{1/2}} + \frac{1}{J_K}$$

$$B = 0.62nFC_0D_0^{2/3}V^{-1/6}$$

where J is the measured current density, J_K and J_L are the kinetic and limiting current densities, ω is the angular velocity of the disk, n is the electron transfer number, F is the Faraday constant (96485 C/mol), C_0 is the bulk concentration of O_2 (1.2×10^{-6} mol/cm^3), D_0 is the diffusion coefficient of O_2 in 0.1 M KOH (1.9×10^{-5} cm^2/s), and V is the kinematic viscosity of the electrolyte (0.01 cm^2/s).

The hydrogen peroxide yield (H_2O_2%) and average electron transfer number based on RRDE

measurements can be determined by the following equations:

$$H_2O_2(\%) = 200 \times \frac{\frac{I_r}{N}}{I_d + \frac{I_r}{N}}$$

$$n = 4 \times \frac{I_d}{I_d + \frac{I_r}{N}}$$

where I_d is the disk current, I_r is the ring current, and N is the ring collection efficiency determined to be 0.424.

Computational methods

All calculations were completed within the spin-unrestricted density functional theory (DFT) method, which was implemented in DMol3 package. The generalized-gradient approximation (GGA) with the Becke-Lee-Yang-Parr (BLYP) function was adopted to describe the exchange and correlation effects. The double numerical plus polarization (DNP) was chosen as the atomic orbital basis set. The effective core potential (ECP) was used to treat the core electrons of all the atoms. During all calculations, the convergence tolerance for energy, force, and displacement convergence was set to 2×10^{-5} Ha, 0.004 Ha/Å, and 0.005 Å, respectively. For the relative energy calculation in the electron transfer reaction, we used the method proposed by Nørskov et al. (J. Phys. Chem. B 2004, 108: 17886-17892), who demonstrated that the chemical potential for the reaction ($H^+ + e^-$) can be related to that of $1/2H_2$ in the gas phase by the use of the standard hydrogen electrode. In order to explore the adsorption stability of ORR species on catalyst, the adsorption energy (E_{ads}) was calculated and defined as $E_{ads} = E_{all} - E_{catalyst} - E_{species}$, where E_{all}, $E_{catalyst}$, and $E_{species}$ are the total energies of the catalyst with an adsorbed species, catalyst, and isolated species, respectively. The more negative the adsorption energy, the more stable the adsorption on the catalyst surface.

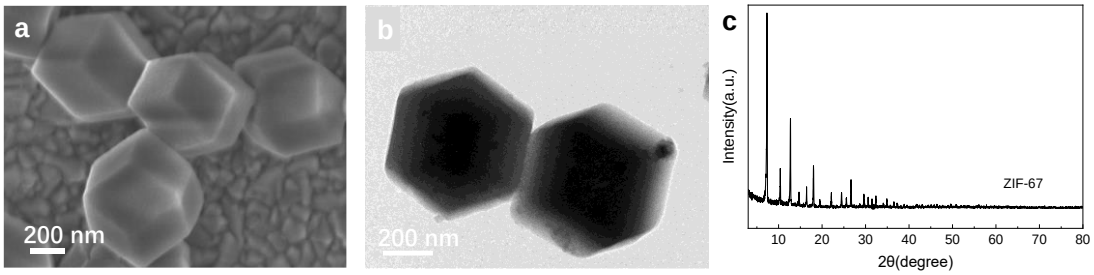

Figure S1. (a) SEM, (b)TEM images, and (c) XRD pattern of ZIF-67.

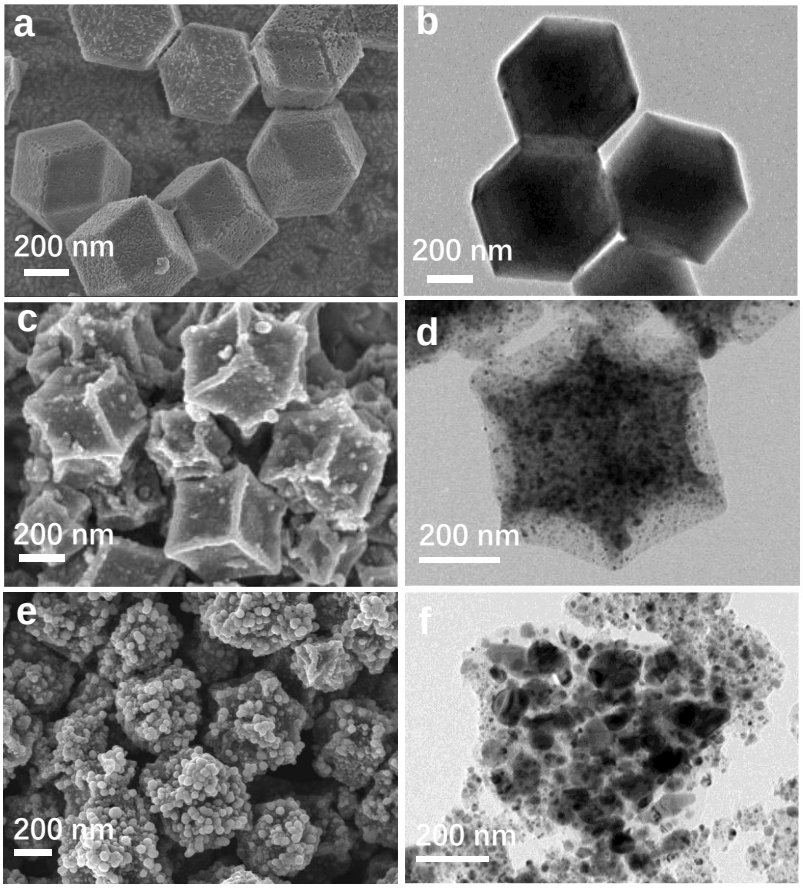

Figure S2. SEM images of (a) Co-SA, (c) S/Co-SA-NP, (e) Co-NP, and TEM images of (b) Co-SA, (d) S/Co-SA-NP, and (f) Co-NP.

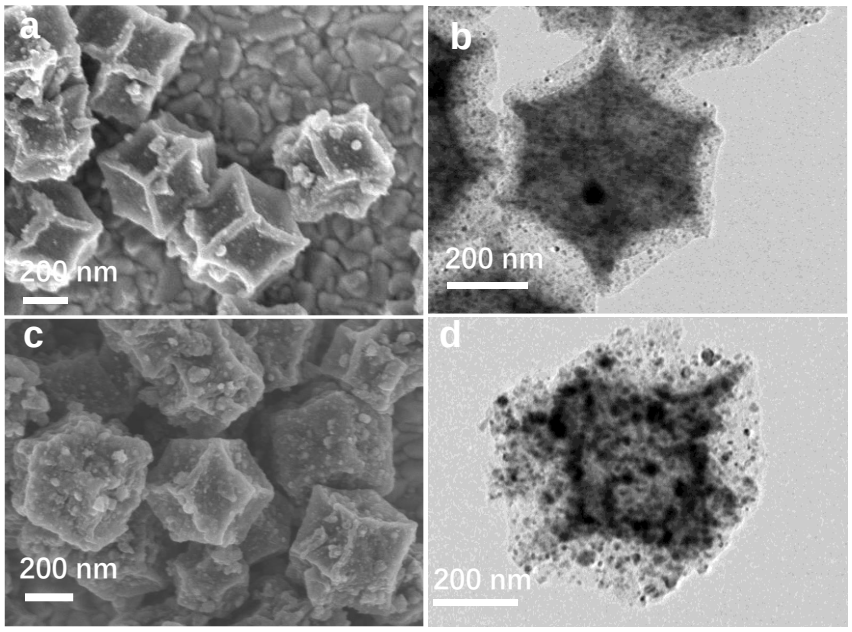

Figure S3. SEM images of (a) Co-700, (c) Co-800, and TEM images of (b) Co-700, (d) Co-800.

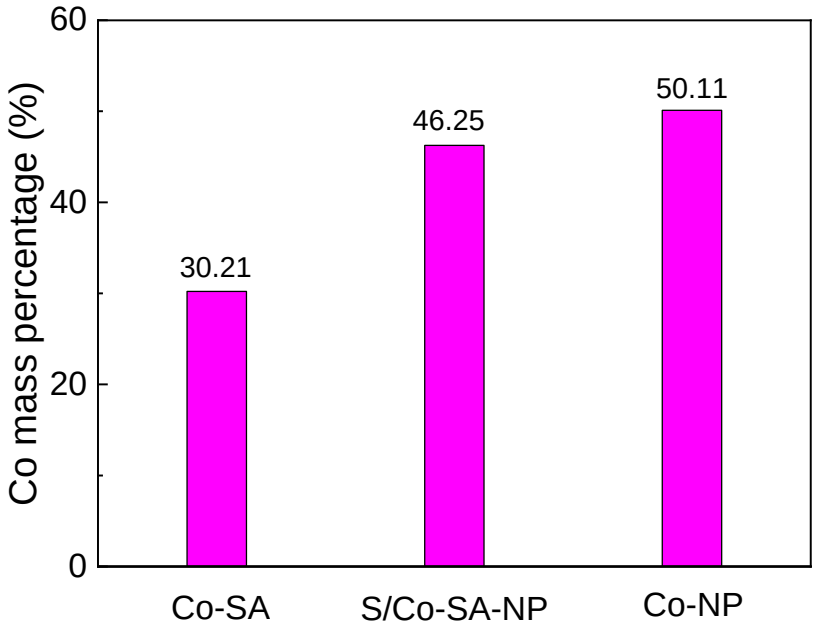

Figure S4. The Co metal mass percentage (%) in Co-based catalysts.

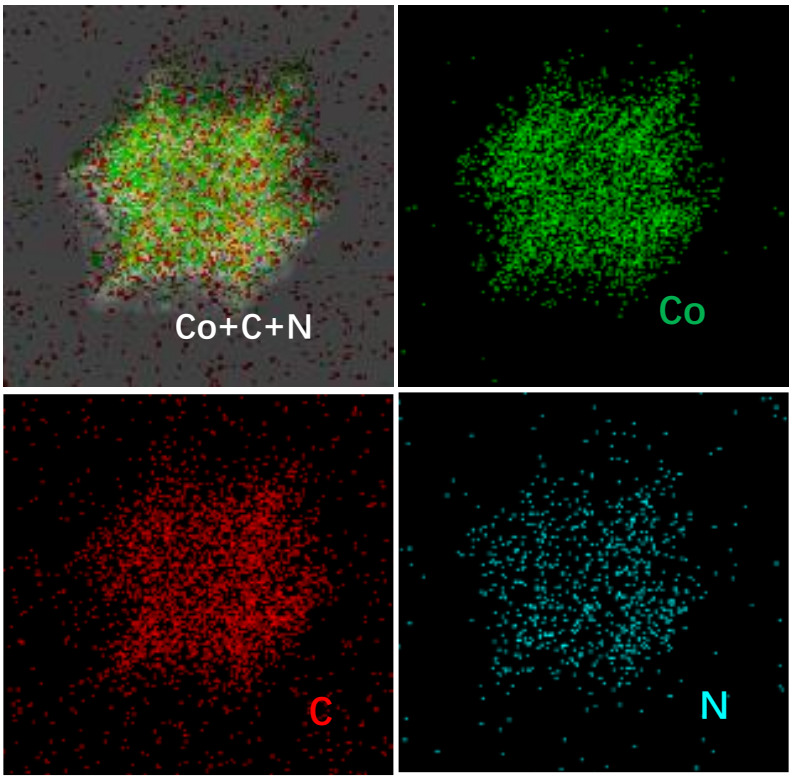

Figure S5. TEM-EDS mapping images for S/Co-SA-NP.

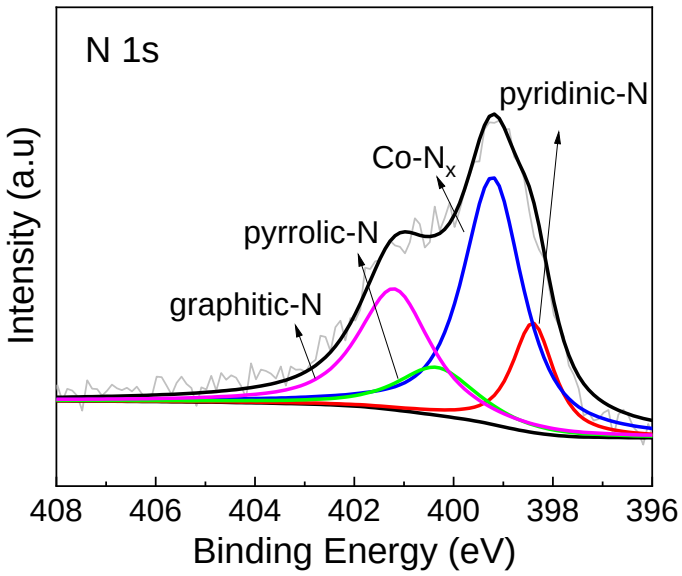

Figure S6. XPS N 1s spectra of S/Co-SA-NP.

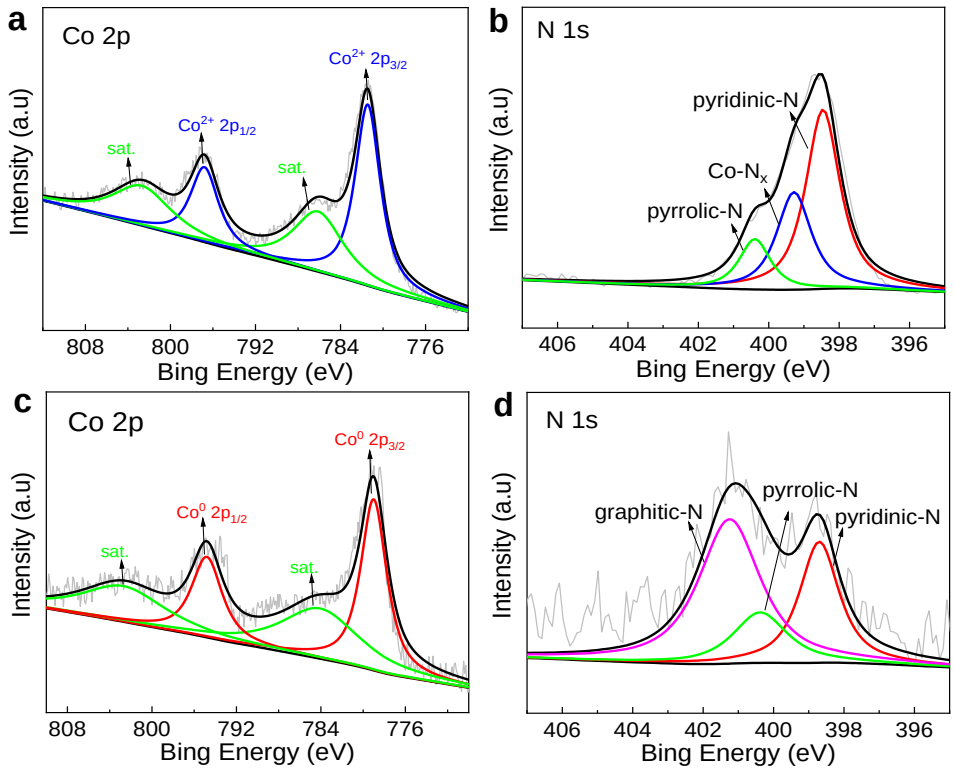

Figure S7. (a) XPS Co 2p spectra, (b) XPS N 1s spectra of Co-SA; (c) XPS Co 2p spectra, (d) XPS N 1s spectra of Co-NP.

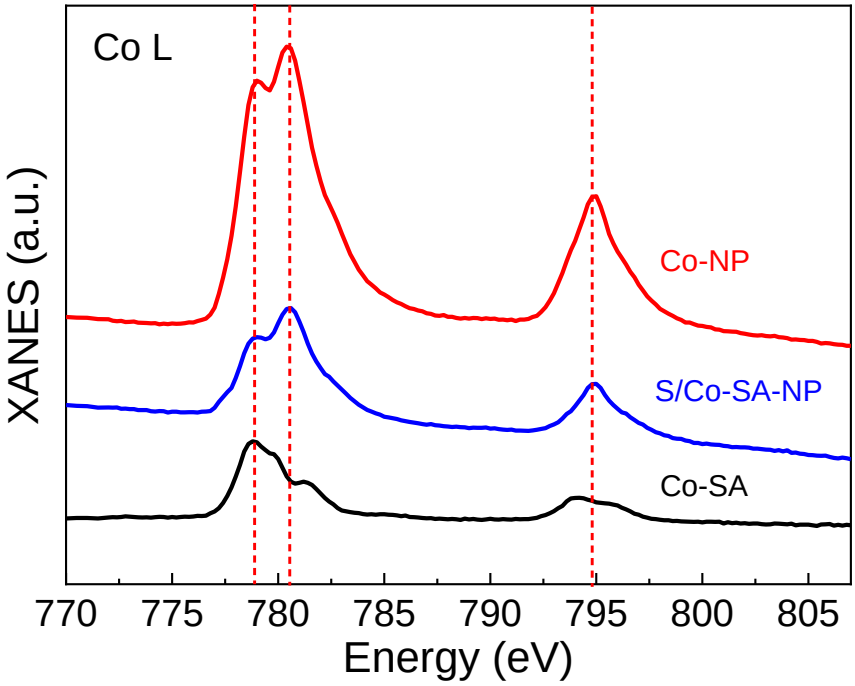

Figure S8. The XANES curves of Co-SA, S/Co SA-NP and Co-NP.

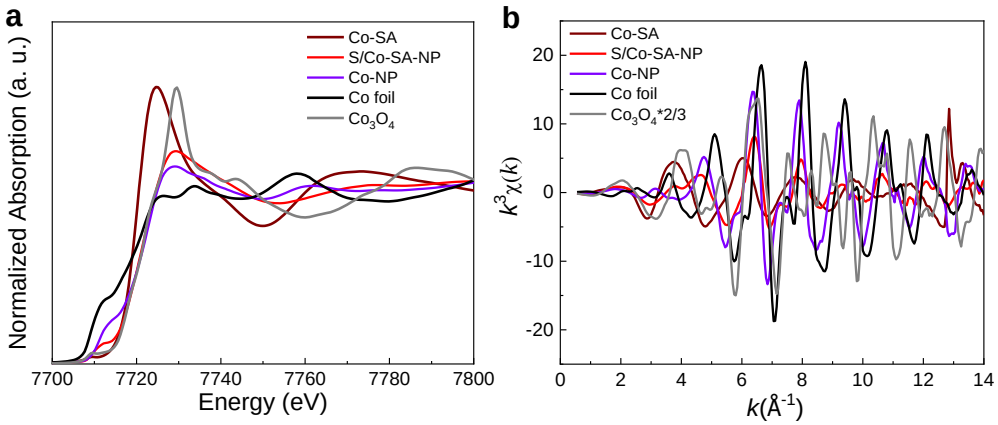

Figure S9. (a) Co K-edge XANES spectra and (b) $k^3\chi(k)$ oscillations.

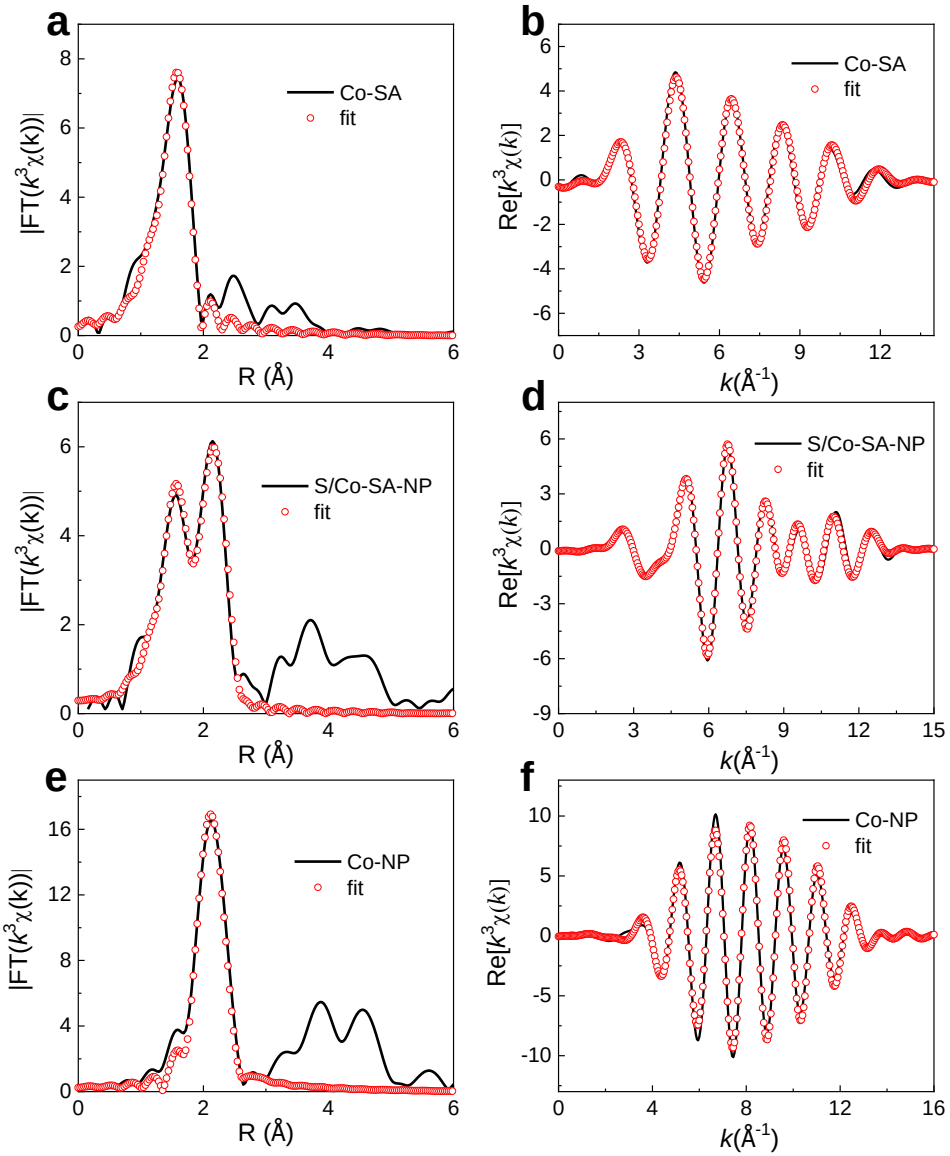

Figure S10. The first-shell fitting of EXAFS spectra Fourier transform (FT) spectra under 0.95 V (a), 0.85 V (c) and 0.70 V (e). The Re($k^3\chi(k)$) oscillation and fitting curves under 0.95 V (b), 0.85 V (d) and 0.70 V (f) for samples.

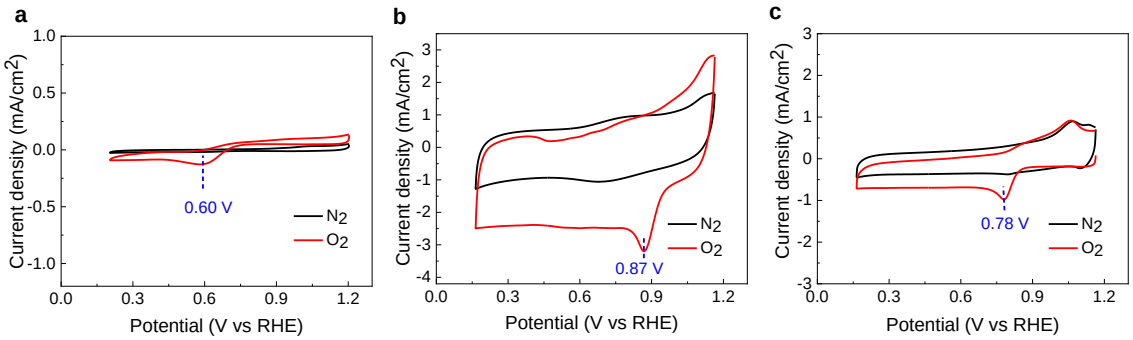

Figure S11. The CV curves of (a) Co-SA, (b) S/Co SA-NP,and (c) Co-NP.

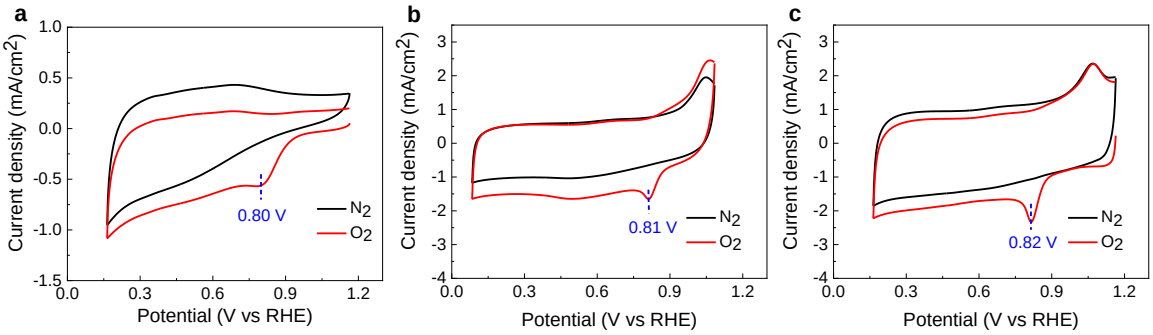

Figure S12. The CV curves of (a) 20%Pt/C, (b) Co-700, and (c) Co-800.

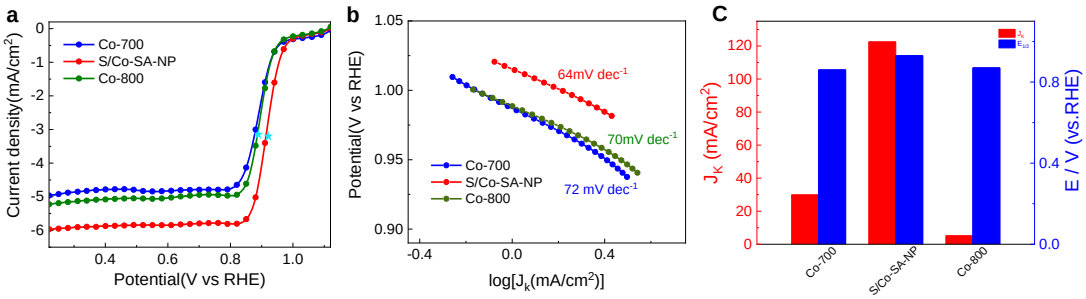

Figure S13. (a) RDE polarization curves, (b) Tafel slopes and (c) J_k and $E_{1/2}$ of Co-700, S/Co-SA-NP and Co-800 in 0.1M KOH.

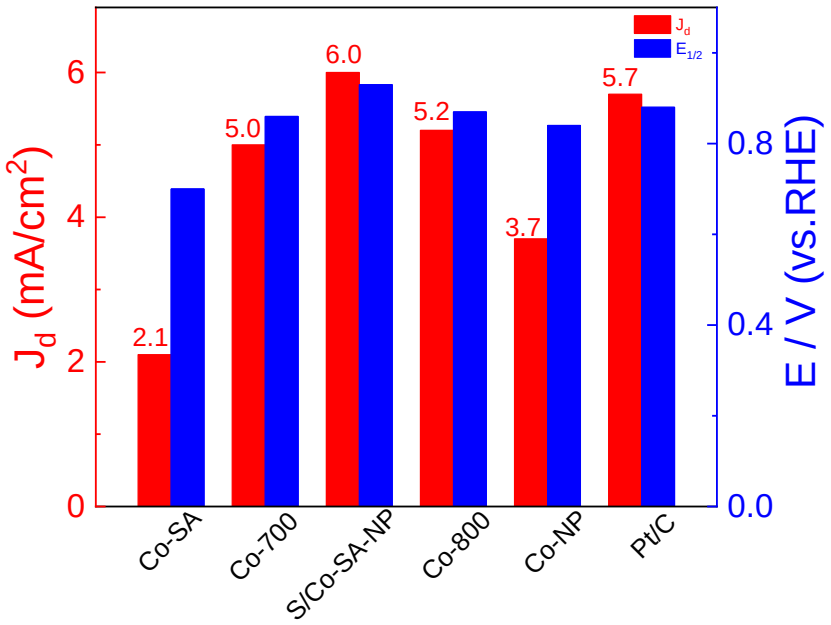

Figure S14. The diffusion limited current density (J_d) and half wave potential ($E_{1/2}$) for different catalysts.

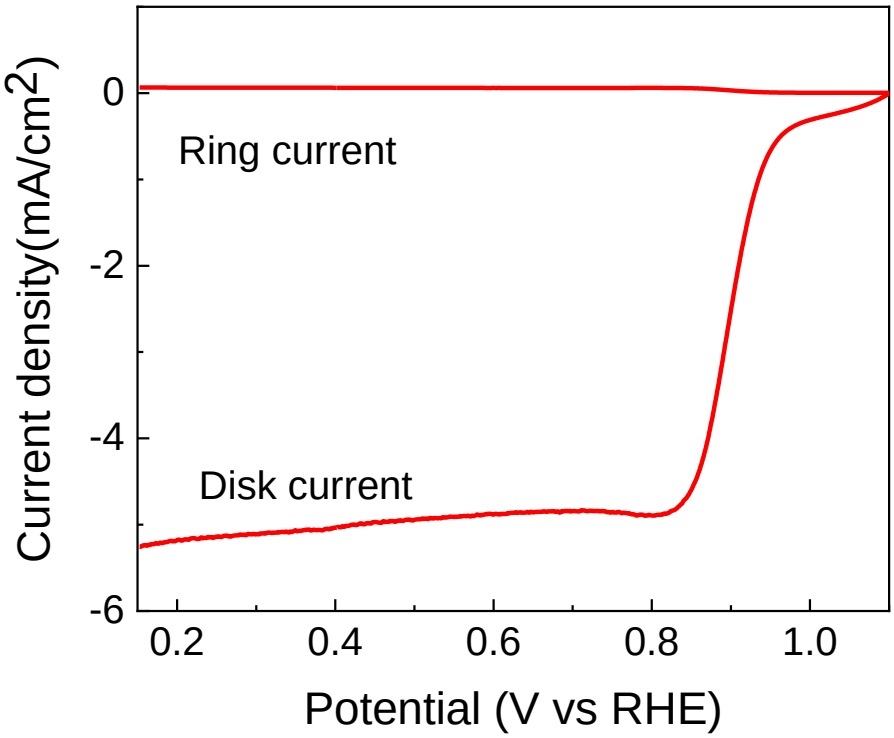

Figure S15. RRDE voltammograms of S/Co-SA-NP in 0.1M KOH.

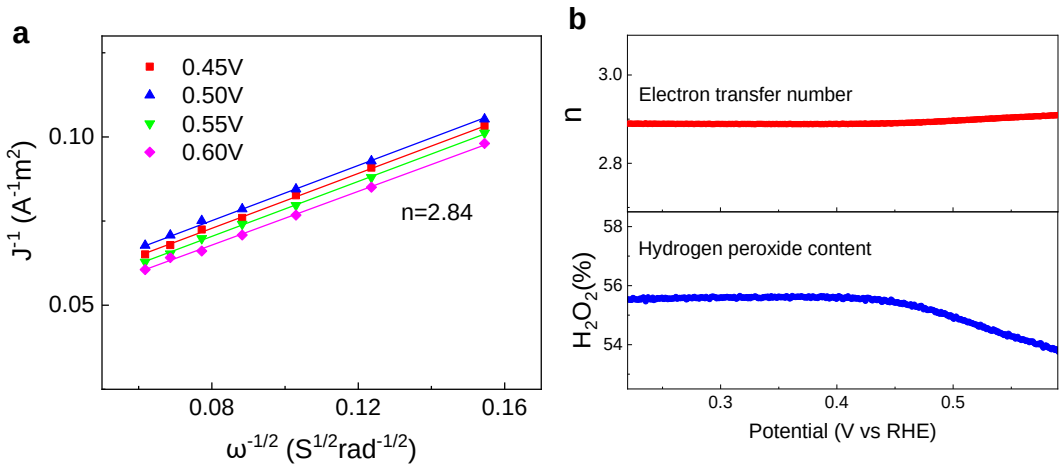

Figure S16. (a) The K-L plots of Co-SA in the range of 0.45– 0.65 V. (b) Electron transfer number (n; top) and H_2O_2 yield (bottom) for Co-SA.

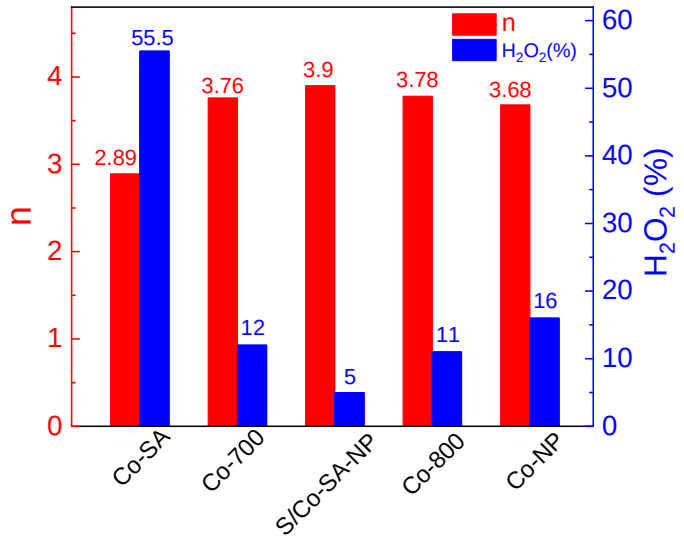

Figure S17. Electron transfer number and H_2O_2 yield of all catalysts.

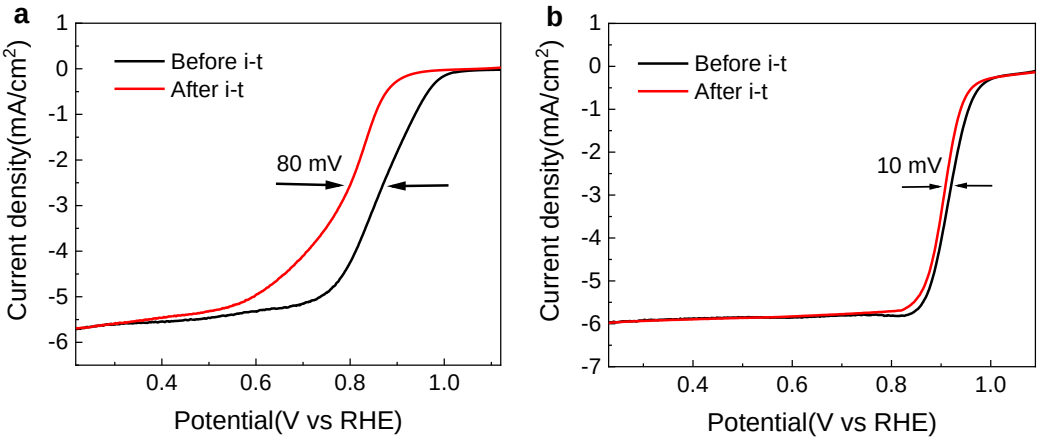

Figure S18. LSV curves of (a) Pt/C and (b) S/Co-SA-NP before and after i-t curves in 0.1 M KOH

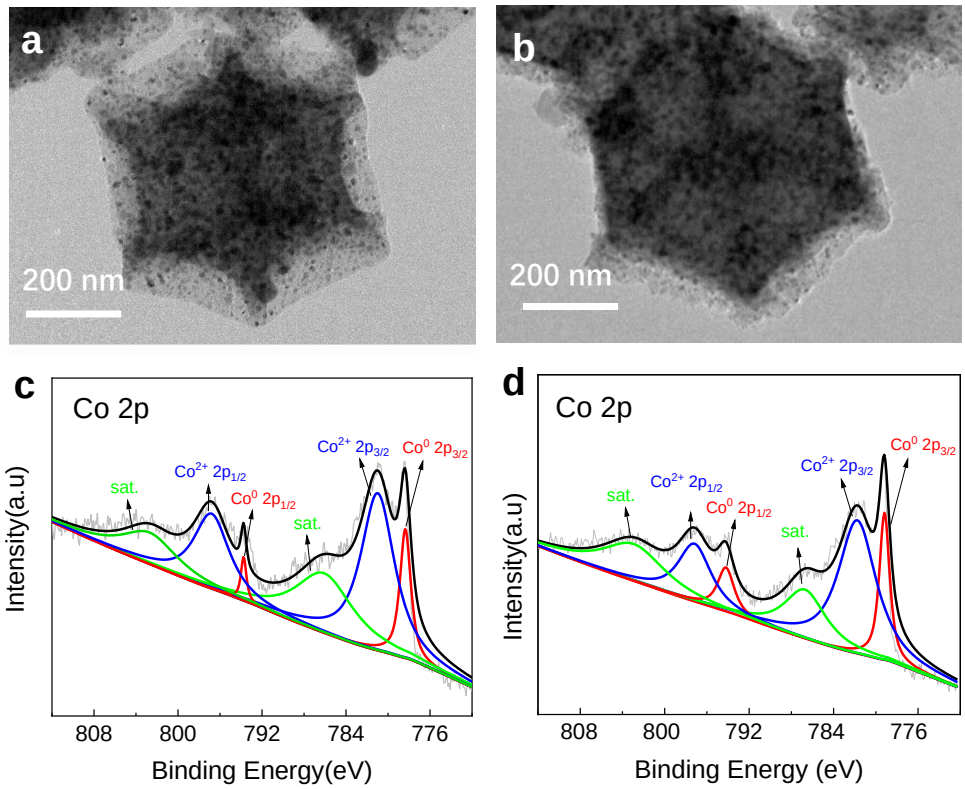

Figure S19. TEM images of S/Co-SA-NP (a) before ORR process, (b) after ORR process; XPS Co 2*p* spectra of S/Co-SA-NP (c) before ORR process, (d) after ORR process.

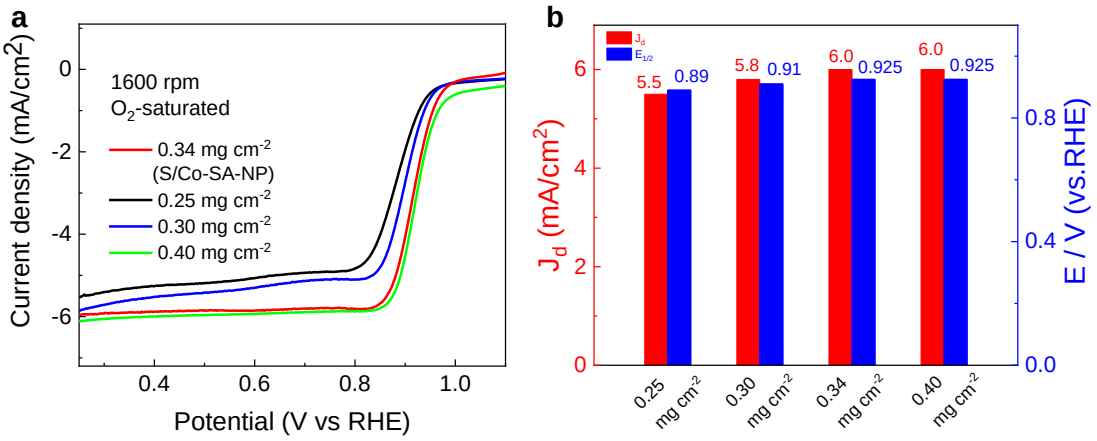

Figure S20. (a) Linear sweep voltammograms (LSVs), (b) Diffusion limited current density (J_d) and half-wave potential ($E_{1/2}$) of different metal loadings at 1600 rpm.

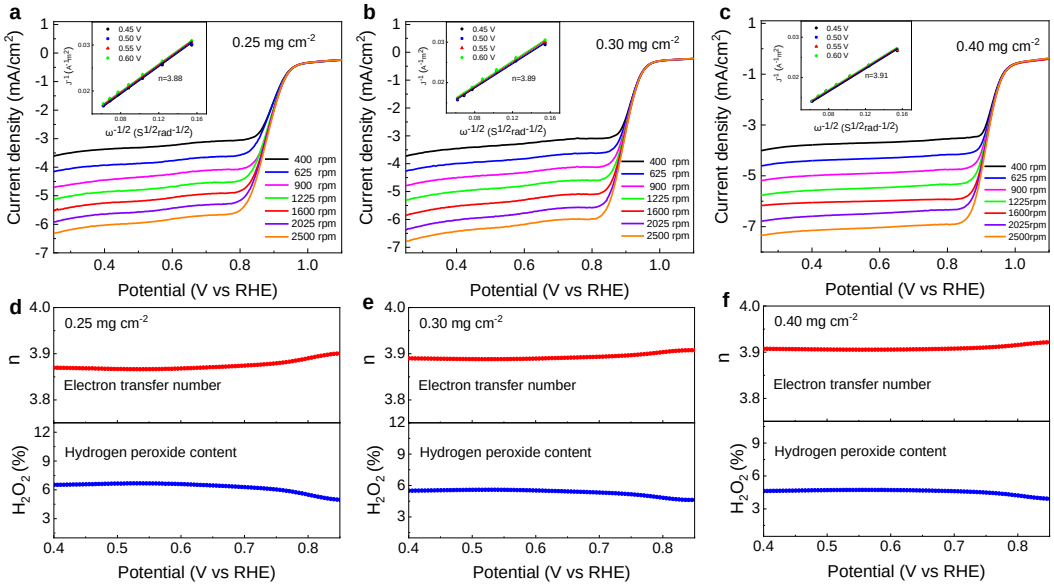

Figure S21. (a), (b), (c) LSV curves of different S/Co-SA-NP loadings at different rotating rates and inset are electron transfer number. (d), (e), (f) the hydrogen peroxide content and electron transfer number for different S/Co-SA-NP loadings.

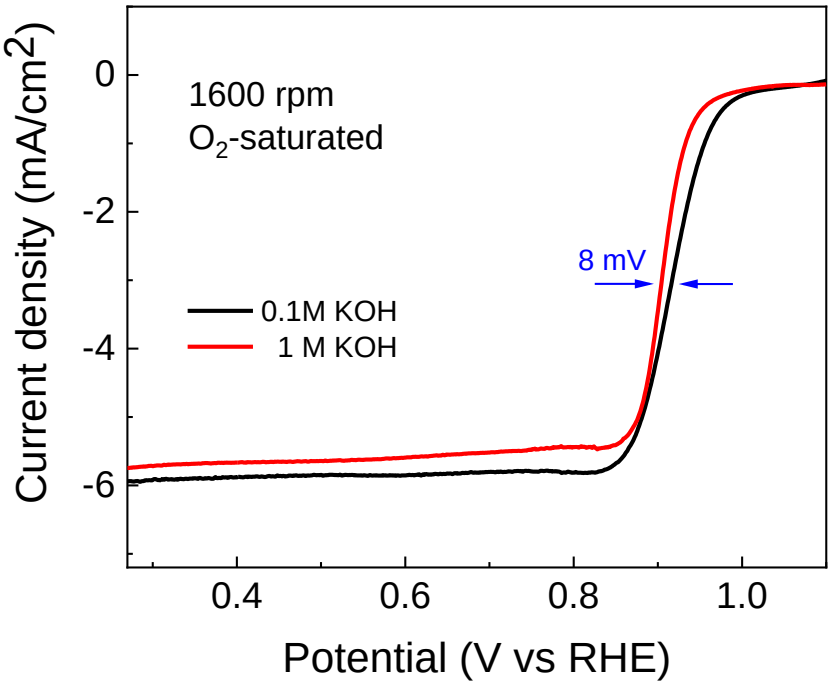

Figure S22. LSV curves of S/Co-SA-NP in different concentrations of KOH.

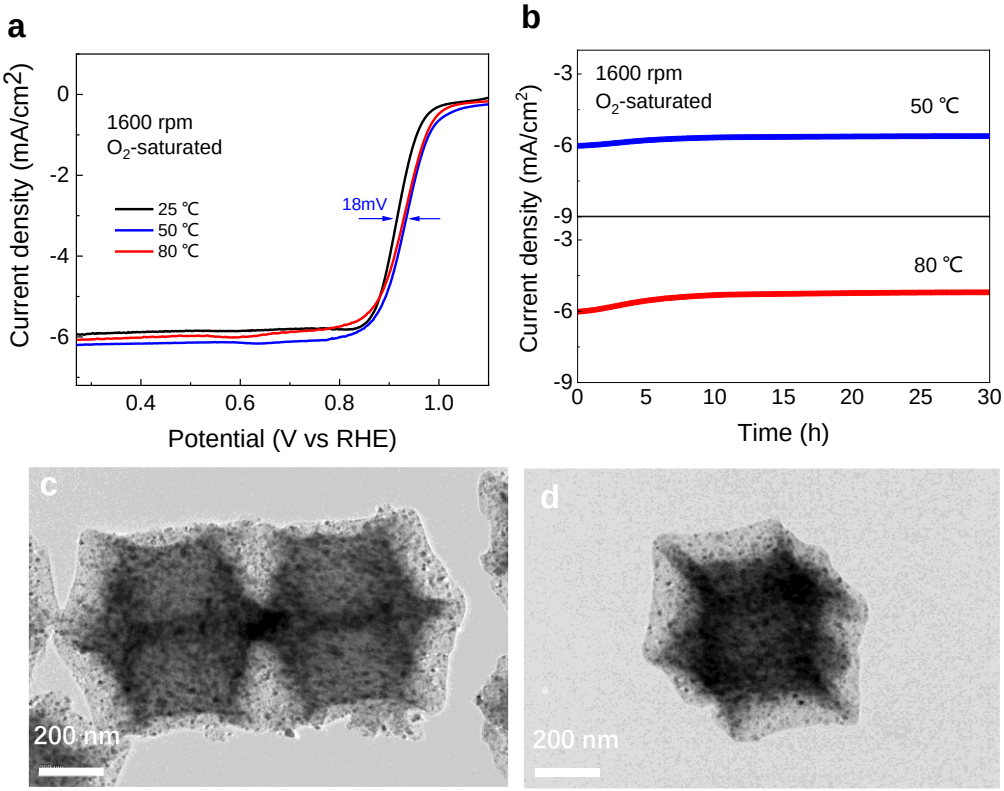

Figure S23. (a) LSV curves of S/Co-SA-NP at different temperatures. (b) Stability tests for S/Co-SA-NP at temperatures of 50 and 80°C. TEM images for S/Co-SA-NP after reaction under 50°C (c) and 80°C (d).

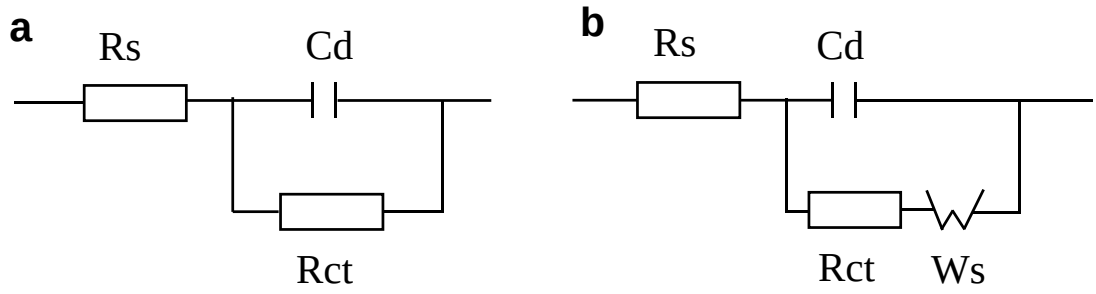

Figure S24. The equivalent circuits of ORR. (a) kinetic control region; (b) potential region with diffusion control.

Table S1. Structural parameters extracted from quantitative EXAFS curve-fitting of samples using the ARTEMIS module of IFEFFIT**.**

Sample	Path	N	R (Å)	σ^2 (10^{-3} Å^2)	ΔE (eV)	R
Co-SA	Co-N	4.1 (±0.1)	2.05 (±0.01)	7.2 (±0.1)	-4.0 (±0.2)	0.009
S/Co-SA-NP	Co-N	2.9 (±0.2)	1.96 (±0.01)	6.2 (±0.1)	-3.6 (±0.2)	0.005
	Co-Co	3.2 (±0.1)	2.50 (±0.01)	9.2 ±0.1)	-2.0 (±0.2)	
Co-NP	Co-Co	4.9 (±0.2)	2.49 (±0.01)	5.4 (±0.1)	-5.0 (±0.2)	0.007

Table S2. Comparison of performance for S/Co-SA-NP in 0.1 M KOH solution, as well as other catalysts reported in the literatures.

Catalysts	$E_{1/2}$(V vs. RHE)	Kinetic current density (J_k, mA cm^{-2})	Tafer slop (mV dec^{-1})	Reference
S/Co-SA-NP	0.925	122.57 at 0.85V	64	This work
Ni2-NC (GC)	0.92	56.2 at 0.8V	67	1
Fe-Nx/C	0.837	10.3 at 0.8V	--	2
Fe@C-FeNCs-2	0.899	41.6 at 0.8V	68	3
Co SAs/N-C(900)	0.881	21.2 at 0.8V	75	4
Co/Co_3O_4@PGS	0.89	--	52.6	5
(Fe,Mn)-N-C	0.9	36.8 at 0.8V	--	6
Co,N-PCL	0.846	--	47.8	7
N.S,O-OMC	<0.75	3.8 at 0.75V	--	8
NOSC8-900	0.74	25 at 0.60V	40	9
Fe-N-C/N-OMC	0.93	57.4 at 0.85	75	10
M/FeCo-SAs-N-C	0.851	32 at 0.8	83	11

Table S3. The fitted parameters of the EIS data of Co-SA catalyst.

Catalyst	Potential(V)	Rs(Ω)	Cd(F)	Rct(Ω)	Ws($S•s^{0.5}$)
Co-SA	0.875	1.799	0.000292	3743	--
	0.85	1.799	0.000291	3267	--
	0.825	1.796	0.00029	2372	--
	0.8	1.794	0.000289	932.3	0.000807
	0.775	1.793	0.000287	764.5	0.003561
	0.75	1.851	0.000172	692.3	0.009951
	0.725	1.851	0.000173	422.7	0.02359
	0.7	1.851	0.000175	272.7	0.04097
	0.675	1.852	0.000178	183.5	0.05997
	0.65	1.85	0.000182	124.7	0.1053
	0.6	1.853	0.000192	74.09	0.09384
	0.55	1.866	0.000223	80.78	0.05458
	0.5	1.886	0.000262	75.69	0.01841

Table S4. The fitted parameters of the EIS data of S/Co-SA-NP catalyst.

Catalyst	Potential(V)	Rs(Ω)	Cd(F)	Rct(Ω)	Ws($S•s^{0.5}$)
S/Co-SA-NP	1	1.914	0.005186	504.2	--
	0.975	1.918	0.004993	495.3	--
	0.95	1.920	0.004884	483.8	--
	0.925	1.923	0.00483	435.5	--
	0.9	1.923	0.004805	302.7	--
	0.875	1.917	0.00463	128.6	0.009951
	0.85	1.904	0.004256	25.62	0.02359
	0.825	1.893	0.004107	18.81	0.04097
	0.8	1.890	0.004308	15.45	0.05997
	0.775	1.877	0.004683	14.64	0.1053
	0.75	1.860	0.00539	16.03	0.1184

References

[1] Su H, Zhou W, Zhang H, et al. Dynamic Evolution of Solid-Liquid Electrochemical Interfaces over Single-Atom Active Sites.J. Journal of the American Chemical Society, 2020, 142,12306-12313.

[2] Ramaswamy, N.; Tylus, U.; Jia, Q.; Mukerjee, S. Activity descriptor identification for oxygen reduction on nonprecious electrocatalysts: linking surface science to coordination chemistry. J. Am. Chem. Soc. 2013, 135, 15443.

[3]Jiang, W. J.; Gu, L.; Li, L.; Zhang, Y.; Zhang, X.; Zhang, L. J.; Wang, J. Q.; Hu, J. S.; Wei, Z. D.; Wan, L. J., Understanding the high activity of Fe-N-C electrocatalysts in oxygen reduction: Fe/Fe3Cnanoparticles boost the activity of FeNx. J. Am. Chem. Soc. 2016, 138, 3570-3578.

[4] Yin, P.; Yao, T.; Wu, Y.; Zheng, L.; Lin, Y.; Liu, W.; Ju, H.; Zhu, J.; Hong, X.;Deng, Z., Single cobalt atoms with precise N-coordination as superior oxygen reduction reaction catalysts. Angew. Chem., Int. Ed. 2016, 55, 10800-10805.

[5] Jiang Y, Deng Y P, Fu J, et al. Interpenetrating Triphase Cobalt-Based Nanocomposites as Efficient Bifunctional Oxygen Electrocatalysts for Long-Lasting Rechargeable Zn–Air Batteries.J. Advanced Energy Materials, 2018, 8(15):1702900.

[6] Sahraie N R, Kramm U I, Steinberg J, et al. Quantifying the density and utilization of active sites in non-precious metal oxygen electroreduction catalysts.J. Nature Communications, 2015, 6,8618(2015).

[7] Park H, Oh S, Lee S, et al. Cobalt- and nitrogen-codoped porous carbon catalyst made from core–shell type hybrid metal–organic framework (ZIF-L@ZIF-67) and its efficient oxygen reduction reaction (ORR) activity.J. Applied Catalysis B: Environmental, 2019,246,322-329.

[8] Cheon J Y, Kim J H, Kim J H, et al. Intrinsic Relationship between Enhanced Oxygen Reduction Reaction Activity and Nanoscale Work Function of Doped Carbons[J]. Journal of the American Chemical Society, 2014, 136(25):8875-8878.

[9] Meng Y, Voiry D, Goswami A, et al. N-, O-, and S-tridoped nanoporous carbons as selective catalysts for oxygen reduction and alcohol oxidation reactions.J. Journal of the American Chemical Society, 2014, 136(39):13554-13557.

[10] Han J X, Bao H L, Wang J Q, et al.N-Doped Ordered Mesoporous Carbon Supported Single-Atom Iron as a Superior Electrocatalyst for Oxygen Reduction Reactions and Zinc-Air Batteries[J]. Applied Catalysis B: Environmental, 2020, 280(2021):119411.

[11] Yin S H, Yang J, Han Y, et al. Construction of Highly Active Metal-Containing Nanoparticles and FeCo-N_4 Composite Sites for Acid Oxygen Reduction Reaction[J]. Angew. Chem. Int. Ed, 2020.59,21976-21979.